Interplay between Dynamic Heterogeneity and Interfacial Gradients in a Model Polymer Film

Austin D. Hartley,[1] William F. Drayer,[1] Asieh Ghanekarade,[1] and David S. Simmons[1, a)]

[1] *Department of Chemical, Biological, and Materials Engineering, The University of South Florida, Tampa, Florida, 33620, United States of America*

(Dated: 22 July 2024)

Glass-forming liquids exhibit long-lived, spatially correlated dynamical heterogeneity, in which some nm-scale regions in the fluid relax more slowly than others. In the nanoscale vicinity of an interface, glass formers also exhibit the emergence of massive interfacial gradients in glass transition temperature T_g and relaxation time τ. Both of these forms of heterogeneity have a major impact on material properties. Nevertheless, their interplay has remained poorly understood. Here we employ molecular dynamics simulations of polymer thin films in the isoconfigurational ensemble in order to probe how bulk dynamic heterogeneity alters and is altered by the large gradient in dynamics at the surface of a glass-forming liquid. Results indicate that the τ spectrum at the surface is *broader* than in the bulk despite being shifted to shorter times, and yet is less spatially correlated. This is distinct from the bulk, where the τ distribution becomes broader and more spatially organized as the mean τ increases. We also find that surface gradients in slow dynamics extend further into the film than those in fast dynamics - a result with implications for how distinct properties are perturbed near an interface. None of these features tracks locally with changes in the heterogeneity of caging scale, emphasizing the local disconnect between these quantities near interfaces. These results are at odds with conceptions of the surface as reflecting simply a higher 'rheological temperature' than the bulk, instead pointing to a complex interplay between bulk dynamic heterogeneity and spatially organized dynamical gradients at interfaces in glass forming liquids.

[a)] Electronic mail: dssimmons@usf.edu

I. INTRODUCTION

Polymers and other glass-forming materials can exhibit extraordinarily large alterations in dynamics and glass transition temperature in the nanoscale vicinity of interfaces[1–11]. This phenomenon is both practically important in controlling the properties of diverse nanostructured materials[3] and fundamentally important due to its apparent deep connection to the physics of the glass transition[2]. These alterations are dominated by strong dynamical gradients in the vicinity of interfaces[2], representing an immense dynamical heterogeneity that is organized in space and can extend at least $\mathcal{O}(10$ nm) from the interface. The effort to understand these gradients' origins and explicate their connections to the bulk glass transition has been a longstanding challenge in the field.

These immense spatial heterogeneities in dynamics at glass-forming liquid interfaces coexist with bulk dynamical heterogeneity that is well-established to exist far from interfaces in glass forming liquids more generally[12–19]. This heterogeneity takes the form of a distribution of dynamical properties, including segmental relaxation time and cage scale. This distribution is furthermore spatially organized, with a given slow-relaxing particle more likely to be near to other slow-relaxing particles, and vice versa. Bulk dynamic heterogeneity grows on cooling towards the glass transition temperature T_g[16,18,19], is at least partially responsible for the stretched (non-Maxwell) nature of relaxation in glass-forming liquids[20], and is commonly identified as an origin of anomalous decouplings between distinct dynamical properties near T_g[21]. Moreover, some theoretical frameworks identify dynamic heterogeneity as playing a causal role in the glass transition[22,23], although this proposition remains unsettled.

A significant point of interest in the study of nanoconfined glass-forming liquids has thus been the question of whether and how dynamic heterogeneity is altered under nanoconfinement. It has even been suggested that alterations in dynamic heterogeneity may play a mechanistic role in dynamical alterations near interfaces[24]. Indeed, multiple theoretical efforts to predict glass formation behavior near interfaces invoke dynamical heterogeneity and surface alterations in heterogeneity or the percolation of heterogeneous domains[25–27]. This issue is extremely challenging to probe in both simulation and experiment, however, due to the difficulty of quantifying the breadth and spatial organization of the relaxation spectrum in a depth-dependent manner.

Here we employ simulations of thin polymer films in the isoconfigurational ensemble[14] in

order to visualize and quantify alterations in dynamic heterogeneity near the surface of a polymer film. Simulations in the isoconfigurational ensemble average over many potential velocities emanating from a single point in configuration space; they thus allow the calculation of quantities that are normally defined only at an ensemble level at a spatial resolution of a single particle in the simulation. In prior simulation work, this capability has been employed to probe the nature of dynamic heterogeneity and its connection to various glassy properties in unparalleled detail[13,14,20,28].

Results of these simulations point towards a nontrivial interplay between interface effects and bulk dynamic heterogeneity. We find that surface alterations of slow dynamics persist over a longer range than surface alterations of fast dynamics. This may have implications for experimental measures of the surface range, indicating that results may depend on the moment of the relaxation spectrum probed. Moreover, rather than simply shifting the entire relaxation spectrum to shorter times, we find that proximity to an interface dramatically alters the form of this spectrum, driving emergence of a massive excess wing of fast dynamics in addition to shifting the spectrum to shorter times. Conversely, we find that this broadened distribution actually becomes *less* spatially correlated near the free surface, contrary to what would be intuited from the bulk behavior. This complexity is also quite distinct from what we observe in the segmental caging scale, the distribution and spatial correlations of which are relatively weakly perturbed near the free surface. Finally, results show that the interface drives emergence of an appreciable local dynamic anisotropy, with in-plane motion favored over out of plane motion for segments adjacent to the interface. This anisotropy is fairly weak at short times and becomes increasingly more pronounced with increasing time of motion – a consequence of the reflective nature of the surface boundary condition for dynamics.

II. SIMULATION METHODS

A. Simulated system and thermal history

We study spatial correlations in dynamics within molecular dynamics simulations of a bead-spring polymer film, supported on a substrate that is nearly dynamically neutral. We employ a variation of the bead-spring model of Kremer and Grest[29], with this variant introducing attractive interactions and employing a reduced bond length so as to improve

resistance to crystallization in the presence of a crystalline substrate[30].

Sub-entangled bead-spring polymer chains of length 20 are simulated in a film configuration, in contact with a crystalline substrate in which the polymer-wall interaction potential is tuned to yield nearly no perturbation, relative to bulk, of the local dynamics, as in our recent work[31]. This leaves the free surface as the only interface in the system that induces large dynamical alterations, allowing study of this surface gradient with minimal interference from substrate effects. The films simulated in this system are $\sim 30\sigma$ (~ 30 nm in real units) thick, and are wider than they are thick so as to eliminate any lateral finite-size effect. Simulations are performed in LAMMPS[32] and employ a Nose-Hoover thermostat with a damping parameter of 2 τ_{LJ} (where τ_{LJ} is the Lennard Jones unit of time and is roughly equivalent to 1 ps) for temperature control. Simulations are nominally performed in the NVT ensemble, but the presence of a free surface yields effective NPT film behavior.

Equilibrium configurations at temperatures in the glass-formation range are produced via a thermal quench process following the previously described PreSQ protocol[33]. We select two of these temperatures, T = 0.431 and T = 0.450, as the focus of the isoconfigurational ensemble simulations reported in this study. These systems are isothermally annealed for at least 10 times the segmental relaxation time of the corresponding bulk system at each of these temperatures in order to ensure access to equilibrium segmental relaxation behavior[33]. These temperatures correspond to conditions at which the mean midfilm (nearly bulk-like) segmental relaxation time is $10^{2.6}\tau_{LJ}$ and $10^{3.2}\tau_{LJ}$, respectively, where τ_{LJ} is the Lennard Jones unit of time and is equal to approximately a picosecond. These temperatures are in the supercooled liquid range; study of lower temperatures was precluded by the immense computational cost of running 1000 replicas to greater timescales.

Beginning with these configurations, we then perform simulations in the isoconfigurational ensemble, which is an established approach that permits computation of properties at a single particle level that are normally only defined at the ensemble level[14]. To do so, we make 1000 copies of the equilibrium configurations at each of these two temperatures. Each of these copies is then assigned a new, random set of particle velocities drawn from the Maxwell-Boltzmann distribution at its temperature. Each of these 1000 simulations is then continued as normal, with data collection beginning immediately and with configurations saved exponentially in time. Each individual particle's behavior can then be averaged over these 1000 thermal replicas, with the ensemble average reflecting the mean behavior of a

particle starting in a given location, but with a randomized velocity. This avoids the need for any temporal or spatial averaging. The results of this analysis thus reveal the degree to which the system's spatial configuration encodes a propensity for yielding the ensuing dynamical behavior.

B. Simulation analysis

We compute several dynamical quantities as measures of the relaxation behavior and heterogeneity of these systems.

First, we quantify translational relaxation based on the self-part of the intermediate scattering function,

$$F_s(\boldsymbol{q}, t) = \frac{1}{N} \sum_{j}^{N} \langle \exp\left[-i\boldsymbol{q} \cdot (\boldsymbol{r}_j(t) - \boldsymbol{r}_j(0))\right] \rangle, \tag{1}$$

where $\boldsymbol{r}_j(t)$ is the position of particle j at time t, and $\boldsymbol{q}$ is the wavenumber. When computing an average relaxation time for the whole system as in a standard (not isoconfigurational ensemble), N is the number of particles in the system, and an average is often taken of a series of distinct initial times as well. Here, when computing this quantity in the isoconfigurational ensemble, N instead corresponds to the number of replicas within the isoconfigurational ensemble (1000 in our case), such that the average is performed *separately for each particle* by averaging over its 1000 replicas. The definition above is written for a single wavevector; we further average over many wavevectors of equivalent wavenumber to arrive at the self-part of the intermediate scattering function computed at a scalar wavenumber $q = 7.07196$, corresponding approximately to the first peak of the structure factor. When computing isotropically averaged relaxation, we arrive at this quantity by average over randomly chosen wavevectors with radial amplitude (in three phase space dimensions) approximately equal to this q. When calculating in-plane relaxation, we average over only those wavevectors that possess approximately this amplitude and that lie in this plane in phase space (for example, for relaxation in the x-y direction we consider only those wave vectors with z-component of zero).

At temperatures in the glass formation range, $F_s(q, t)$ relaxation function obeys a characteristic two-step relaxation, with an initial picosecond timescale relaxation giving way to

the segmental alpha relaxation process. Most commonly, these data are analyzed in simulation by truncating the short time process and then fitting the long-time alpha process to a Kohlsrauch-Williams-Watts stretched exponential. However, the immense particle-to-particle heterogeneity observed in our simulations, together with the need to perform this analysis for every one of 61,200 polymer segments separately, complicates this approach. The relative magnitudes of the picosecond and alpha relaxation, as well as their degree of separation, are highly variable from particle to particle. Usual truncation approaches thus often miss important components of the relaxation process, identification of parameter guesses that lead to good convergence across all particles is nearly impossible, and manual adjustment of the fit is impractical.

To resolve this, we employ a multi-step fitting procedure in which we fit the entire self-intermediate scattering function to a two-step decay form, given by

$$F_s\left(q,t\right) = A\exp\left[-\left(\frac{t}{\tau_{fast}}\right)^{\beta_{fast}}\right] + \left(1-A\right)\exp\left[-\left(\frac{t}{\tau_{slow}}\right)^{\beta_{slow}}\right]. \tag{2}$$

Here subscripts of $fast$ and $slow$ denote parameters describing the picosecond process and the slower α process, respectively. We begin by first fitting data at short time to the first of the two stretched exponential terms above. This fit generally recovers a compressed exponential. To select this time range, we find the lowest value of the relaxation function within the time window from $0.1\tau_{LJ}$ to $1.0\tau_{LJ}$. We then fit the first stretched exponential to all times up to this time point.

We then fix the parameters for this first KWW term, and we fit the entire time range of $F_s(q,t)$ to the full equation above, employing only A, τ_{slow}, and β_{slow} as free parameters. Finally, we refit the equation above to the full time data set, leaving all parameters free, but using the parameters from steps 1 and 2 as guesses. We find that this yields good convergence in the overwhelming majority of cases. Most remaining problematic fits are encountered in the immediate vicinity of the substrate, which is not the focus of this study, and we therefore exclude segments in the near-substrate domain (within 5 σ of the substrate) from this analysis. For each particle, once the fit to Eq. 2 is complete, we compute a mean relaxation time as

$$\tau = A\frac{\tau_{fast}}{\beta_{fast}}\Gamma\left(\frac{1}{\beta_{fast}}\right) + \left(1-A\right)\frac{\tau_{slow}}{\beta_{slow}}\Gamma\left(\frac{1}{\beta_{slow}}\right), \tag{3}$$

where Γ is the Gamma function and where this equation reflects the zeroth moment of the fit two-step relaxation function.

We also compute the mean square displacement of each particle versus time by averaging over the square displacements of its 1000 thermal replicas. We then define a characteristic segmental displacement time t^*. This is essentially another metric for a relaxation time. t^* is defined as the time at which a given particle's mean square displacement is equal to $2\pi/7.07196$, which defines a length scale comparable to that implied by the choice of q in the self-intermediate scattering function calculation described above. We additionally extract from the mean-square displacement data the Debye-Waller factor $\langle u^2 \rangle$ for each particle, which we define in a common manner as the value of $\langle r^2 \rangle$ for a given particle when $t = 1\tau_{LJ}$.

III. RESULTS

A. Surface modifications of relaxation time heterogeneity

We begin by exploring how the distribution of segmental relaxation times varies with position near the surface of the film. Figure 1(a) and (b) illustrate scatter plots of the inverse relaxation time of every particle in the upper 25 σ of the film vs its position. This figure makes clear that relaxation systematically and dramatically accelerates upon approach to the surface of the film, with the entire distribution of relaxation times shifting towards faster relaxation.

We analyze this trend more quantitatively by plotting, in Figure 2, the distribution of relaxation times for layers of segments at various distances from the surface. Consistent with our prior work in the isoconfigurational ensemble in the bulk[20], the mid-film relaxation spectrum is asymmetric, with a broad tail of fast relaxation and a relatively sharp dropoff on the slow-relaxing side. Near the film surface, this distribution both shifts to shorter times and appreciably broadens. The broadening is particularly pronounced on the fast side of the spectrum but is not purely asymmetric; there is also appreciable apparent broadening on the slow side of the spectrum.

To confirm that this finding is not unique to the specific measure of relaxation we have employed above, we perform the same analysis for the segmental displacement time t^*. As can be seen in Figure 1(c) and (d), the distribution of t^* is narrower than that of τ, but

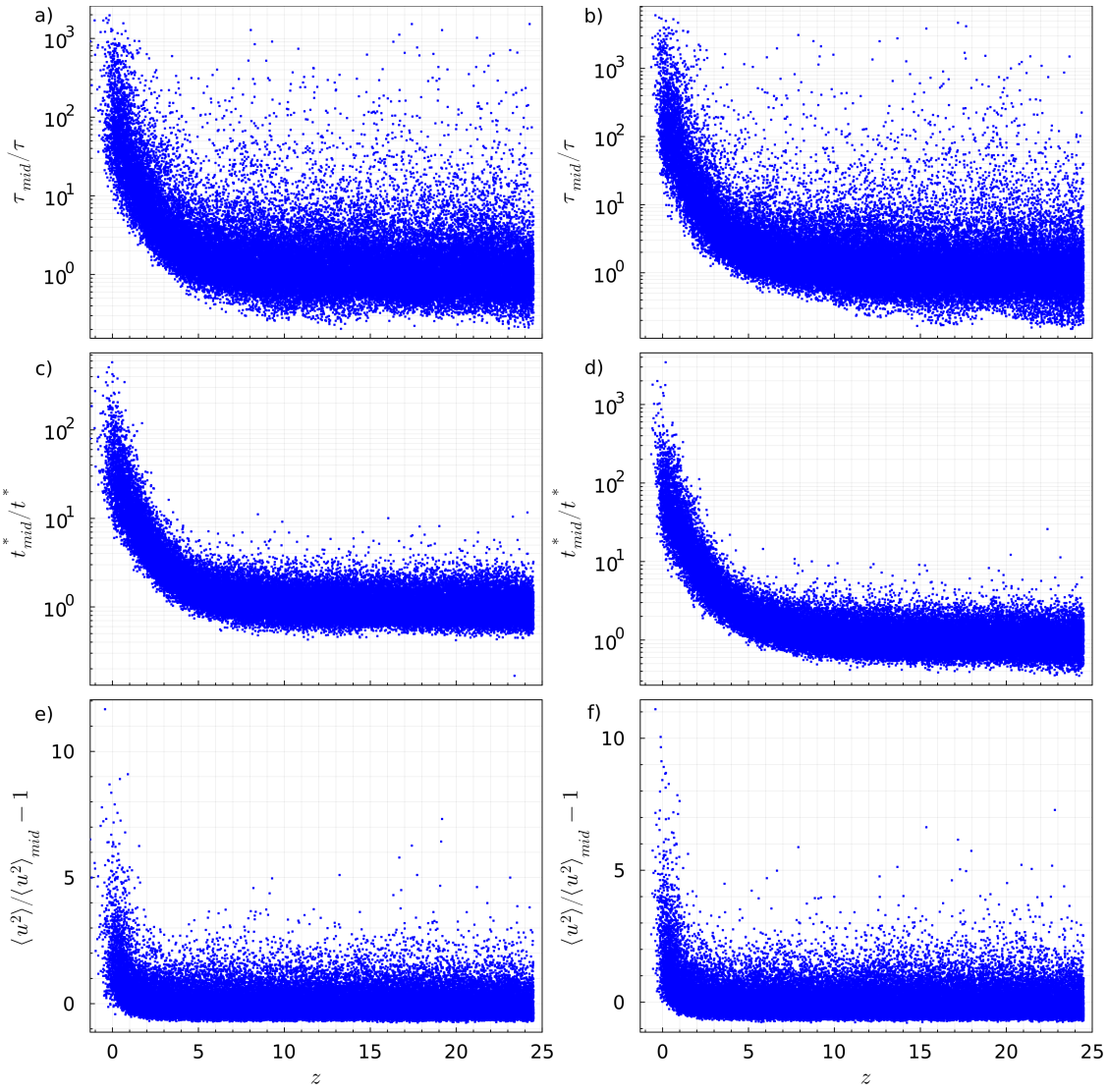

FIG. 1. (a and b) Normalized inverse relaxation time, (c and d) normalized inverse displacement time t^*, and (e and f) normalized excess Debye-Waller factor (relative to the mid-film), plotted vs distance from the free surface of every particle in the upper 25 σ of the film, with single-bead τ values determined in the isoconfigurational ensemble as described in the text. The left column of panels reports data at a temperature $T = 0.431$ while the right column reports data at a temperature of $T = 0.450$.

the variation on approach to the surface is quite similar. As shown in Figure 3, the same basic findings hold for the distribution of t^* as for the distribution of τ values: they shift to shorter times and broaden upon approach to the surface.

In the SI, we show that this observation of a broadened dynamical distribution at the free

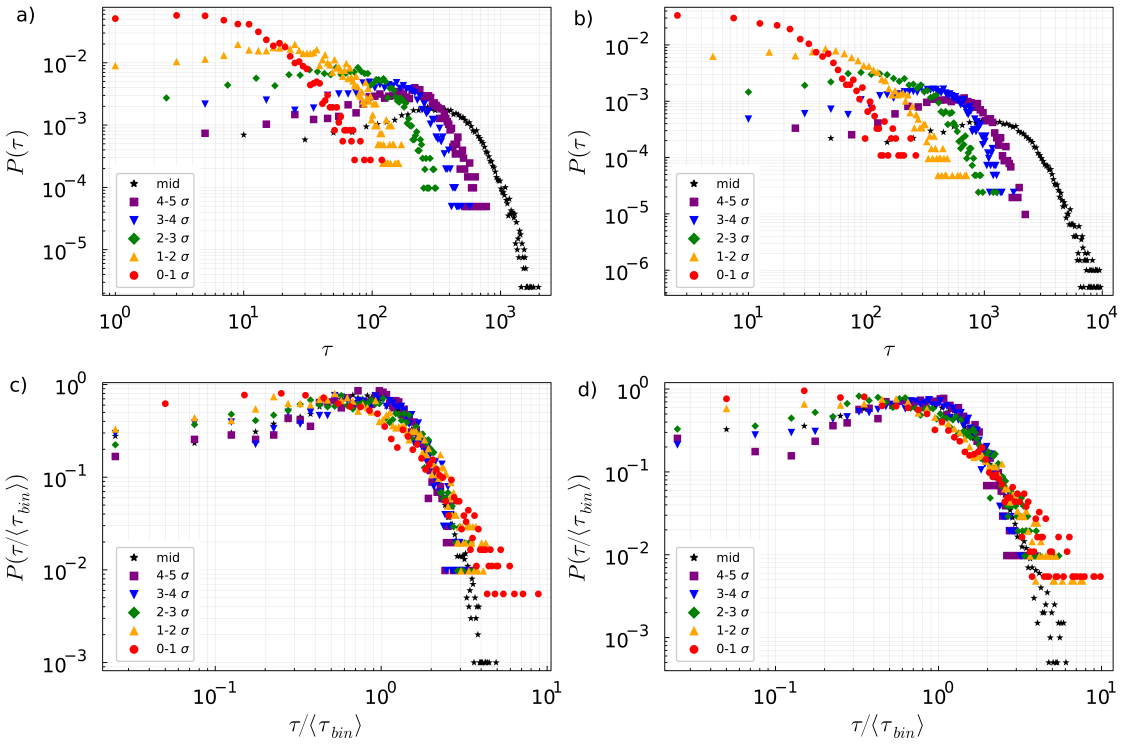

FIG. 2. Distribution of relaxation times for bins of particles at distances from the free surface noted in the legend. The left column of panels reports data at a temperature T = 0.431 while the right column reports data at a temperature of T = 0.450. Panels (c) and (d) report the same values, but for each particle normalized by the mean value in that bin of particles.

surface is qualitatively bin-size independent and is thus not a result of residual averaging over a finite size bin. In other words, this broadening is not a reflection of the presence of averaging over a large gradient in dynamics at the free surface. This indicates that the free surface is genuinely more dynamically heterogeneous, even on an in-plane basis, than the bulk.

This observation of a broader relaxation spectrum at the surface of the film has direct implications for the understanding of dynamics near the free surfaces of glass-forming liquids. A common conception has been that the surface region acts as though it obeys a higher 'rheological temperature' or effective temperature than the bulk[34,35]. The results reported above contraindicate this interpretation. In general, glass-forming liquids become less dynamically heterogeneous on heating, a finding that is both indicated by experimental proxies for heterogeneity and confirmed by bulk simulations in the isoconfigurational ensemble[16,18–20,28]. The 'higher rheological temperature' interpretation of enhanced surface

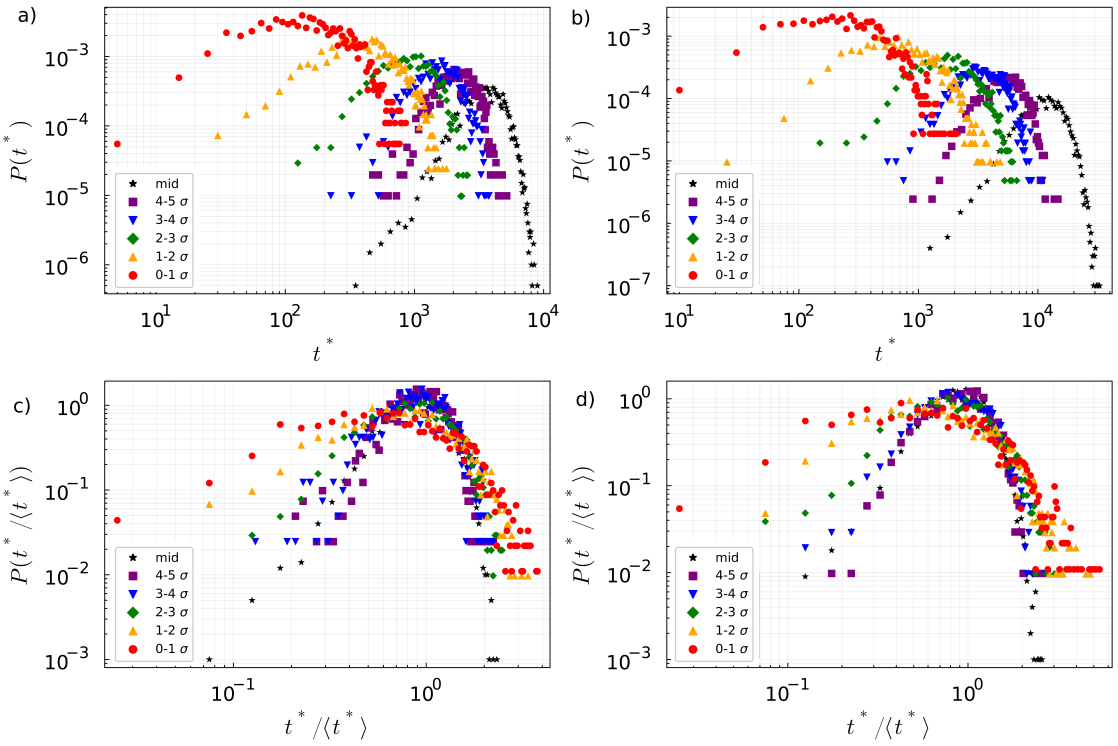

FIG. 3. Distribution of displacement times $t*$ for bins of particles at distances from the free surface noted in the legend. The left column of panels reports data at a temperature T = 0.431 while the right column reports data at a temperature of T = 0.450. Panels (c) and (d) report the same values, but for each particle normalized by the mean value in that bin of particles.

dynamics would thus imply that the surface should be less dynamically heterogeneous than the bulk; however, the opposite is evidently true. In essence, these data indicate that the free surface does not simply 'act as though it were hotter'. Instead, it acts 'hotter' with respect to the mean relaxation time, and 'colder' with respect to the distribution breadth. Evidently, a simple temperature shift of any kind is not the most useful way to conceptualize this situation.

It is evident from the above that the degree of spatial heterogeneity varies near the surface of the film, in a manner that is perhaps unintuitive. A natural question follows: are different components of the relaxation spectrum quantitatively altered more strongly near the surface? For example, are alterations to fast dynamics larger in magnitude or longer ranged than those to slow dynamics, or vice versa? Given that distinct practical mechanical and transport properties reflect distinct moments of the relaxation spectrum, the answer to this question can be expected to mediate how interfaces alter distinct dynamical properties.

To probe this, we compute at each distance z from the surface means reflecting various moments of each dynamical property above. For example, we define a relaxation time reflecting the k^{th} moment of the distribution as

$$\langle \tau(z) \rangle_k = \left[\frac{1}{N} \sum_{i=1}^{N(z)} (\tau_i)^k \right]^{1/k}, \tag{4}$$

where $N(z)$ is the number of particles in a finite-thickness bin of particles at mean distance z from the surface and τ_i is the relaxation time of particle i. Corresponding values are computed for $\langle u^2 \rangle$ and t^* analogously.

As can be seen in Figure 4, a wide range of moments of the τ and t^* distributions obey a double-exponential recovery of bulk values near the free surface. This is consistent with much prior work pointing towards a double-exponential relaxation time gradient over the first $\sim$ 10 nm near a free surface[2,9,31,36–41] and extends this finding to essentially every moment of the translational relaxation spectrum. In order to quantify this spatial variation, we therefore fit the spatial variation at each moment to a double exponential form,

$$\log\left(\frac{\tau_{mid}}{\tau(z)}\right) = A \exp\left(-\frac{z}{\xi}\right) \tag{5}$$

where τ_{mid} is the relaxation time in the middle of the film (an adequate proxy for the bulk relaxation time for these purposes given the thickness of the film), ξ is characteristic decay length scale and A is a magnitude parameter. We analyze t^* gradients via a fit to an analagous form.

As shown in 5, both τ and t^* gradients grow in range with increasing moment of the distribution. Because higher moments weight slower-relaxing parts of the spectrum more heavily, this indicates that slower-relaxing parts of the relaxation time distribution are perturbed further from the interface than are faster relaxing parts of the relaxation time distribution. The τ distribution, unlike the t^* distribution, exhibits a pronounced feature wherein ξ values for negative moments abruptly drop off with decreasing moment, and these values become temperature-independent.

This distinction in the behavior of the τ and t^* at large negative moment k is likely a consequence of the physically and methodologically distinct manner in which we have defined these quantities. t^* reflects merely a timescale necessary to displace a conventional distance, whereas τ reflects a zeroth moment relaxation time obtained from a two-process

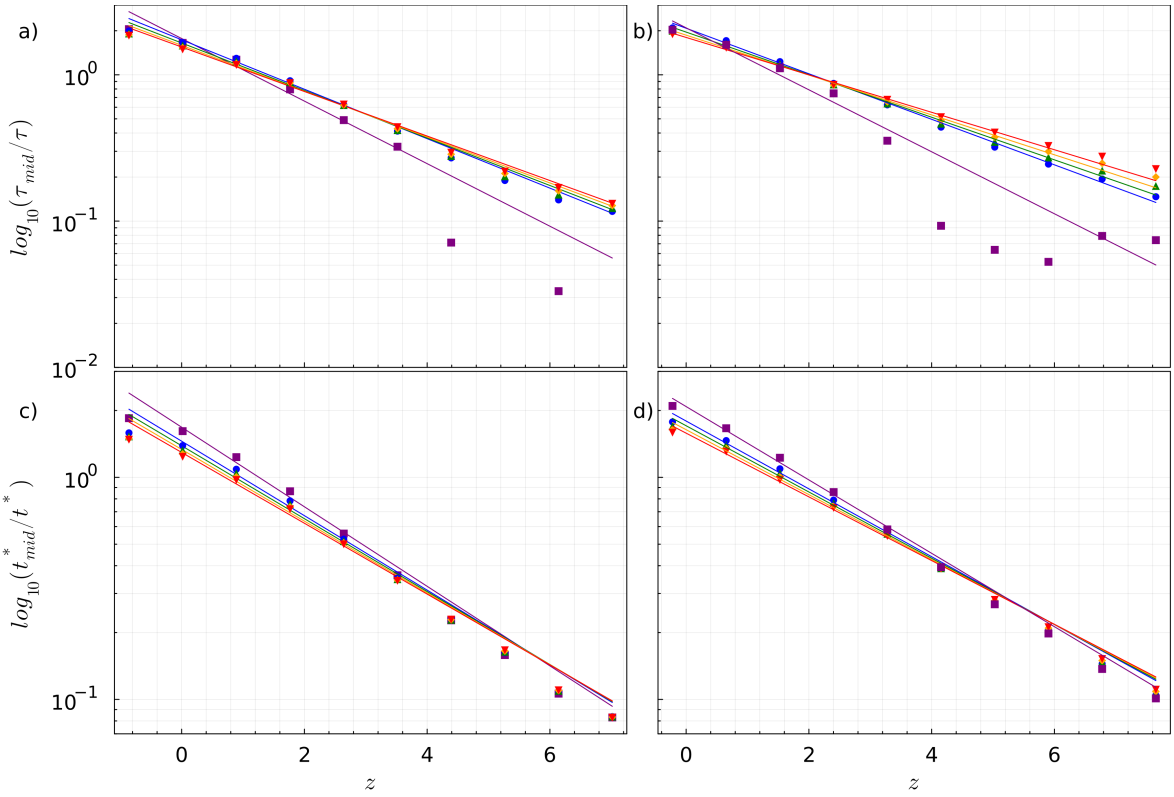

FIG. 4. Local relaxation times (a and b) and displacement times (c and d), computed from distinct moments of their local distributions at a given distance z from the free surface, as described in the text. Moments reported are the -1st moment (purple squares), 1st moment (blue circles), 2nd moment (green triangles), 3rd moment (orange diamonds), and 4th moment (red inverted triangles). The left column (a and c) reports data at a temperature T = 0.431 while the right column (b and d) reports data at a temperature of T = 0.450.

fit to the overall self-part of the intermediate scattering function. Because of the two-process fit employed in extracting a relaxation time from the latter, this quantity reflects both a picosecond β relaxation process and the segmental α process. When the α process is slow, it process totally dominates over the picosecond relaxation process in determining the mean relaxation time. However, when α relaxation time is relatively fast, the mean relaxation time can reflect a mix of the α and picosecond processes, or even become dominated by the picosecond process. We believe that the behavior of negative moments of the τ distribution reflects a portion of the distribution (the fastest relaxing portion) in which the picosecond relaxation dominates over the main α relaxation process. This is consistent with the temperature invariance of this regime, given that the picosecond β process is only weakly

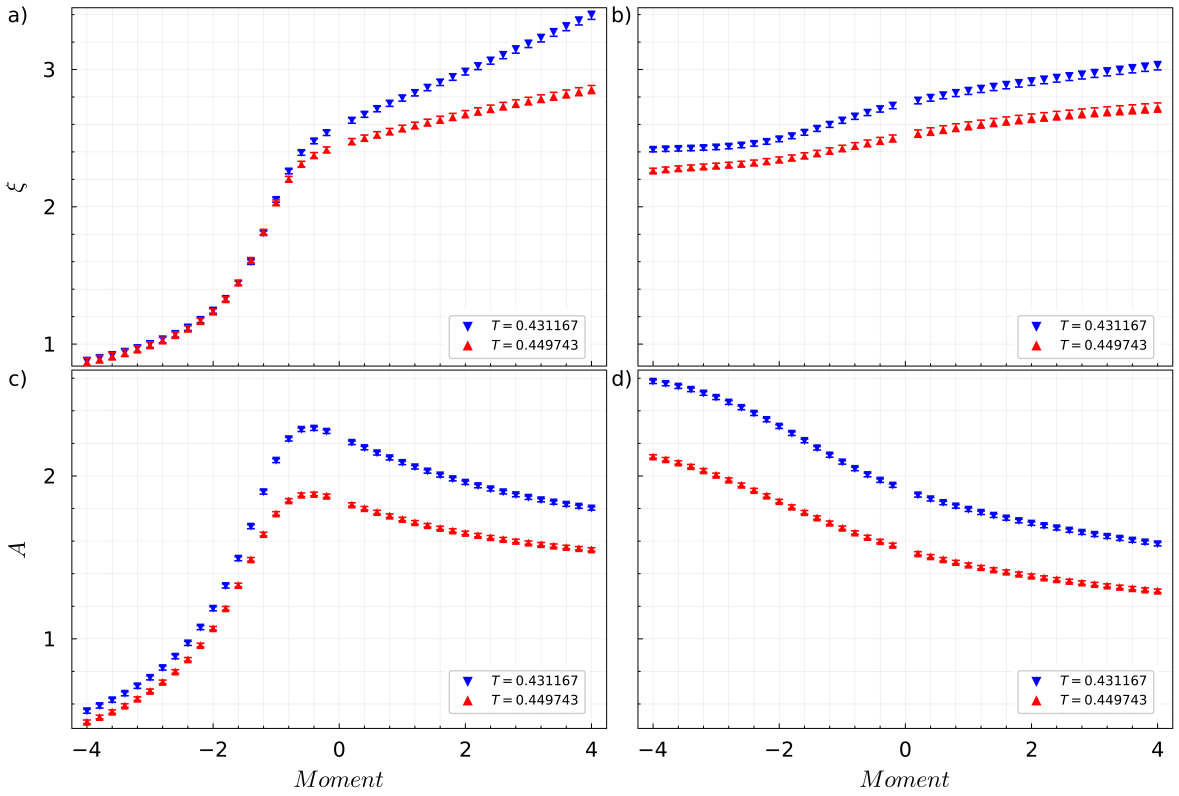

FIG. 5. Range (a) and magnitude (c) of relaxation time gradients $\langle \tau(z) \rangle_k$ as a function of moment, and range (b) and magnitude (d) of displacement time gradients $\langle t^*(z) \rangle_k$ as a function of moment, for the temperatures shown in the legends.

temperature dependent. This feature of the moment-dependence would be expected to shift to even lower moments at lower temperatures, as the mean relaxation time shifts to times that are further removed from the picosecond timescale. Notably, this feature is muted in the t^* distribution, which simply measures time to displace a fixed distance and does not involve a fit to the overall relaxation process. In any case, these two measures of relaxation are consistent in reporting a monotonic increase in the range of the surface perturbation to slower-relaxing parts of the spectrum. Given the reasoning above we focus on this more robust behavior at higher moments in interpreting the effect of the interface on the segmental α process.

Conversely, both t^* and the α-dominated (positive moment) portion of the τ spectrum exhibit a reduction in surface magnitude with increasing moment. Combined with the range trends above, this finding indicates that higher moments (slower relaxing modes) of the spectrum exhibit a surface gradient that is 'smeared out' – longer-ranged but somewhat

attenuated in magnitude – as compared to lower moment (faster relaxing modes).

This has potentially broad implications for understanding property variations near interfaces and under nanoconfinement. Prior studies probing alterations in distinct dynamical properties near free surfaces have often returned seemingly differing results[42–44]. Given that these dynamical properties often probe distinct moments of the relaxation time distribution, the above findings may partially explain these differences, alongside previously studied differences in the way distinct properties average over local gradients in a mean-film measurement[34,35,43–51]. For example, whereas the mean relaxation time probes a forward moment of the relaxation time distribution (i.e. $\langle\tau\rangle$), the diffusion constant probes one over the inverse moment of this distribution (i.e. $1/\langle\tau^{-1}\rangle$)[52]. This difference in moments probed has long been identified as an origin of thermal decoupling between distinct processes in the bulk (exe. "Stokes-Einstein" breakdown of the usual inverse proportionality between viscosity and diffusion rates[52], and the decoupling between chain and segmental modes in polymers[53,54]). Our findings here suggest that surface variations in diffusion and other properties probing low or inverse moments of the relaxation time distribution should be expected to exhibit shorter-ranged gradients at interfaces than viscosities and other properties probing positive or high moments of the relaxation time distribution.

Beyond the question of the change in the breadth of the distribution at the free surface, it is of interest to understand whether *spatial correlations* in mobility are altered near the free surface. Figure 6 depicts a side-view of a simulated film (rendered in VMD[55]), in which beads are colored by their $\log(\tau)$ value. This image emphasizes the coexistence of a spatially heterogeneous gradient of dynamics at the free surface with the more bulk-like heterogeneity that exists in glass-forming liquids more generally. The most visually pronounced feature is the massive gradient in relaxation times at the surface. In parallel to this, there are 'bulk-like' spatially correlated slow and fast domains throughout the film. It is also evident that faster-relaxing domains sometimes interconnect between the surface and buried regions of the film, which might provide pathways for more rapid diffusion across the film via the surface layer.

Assessment of alterations in the more 'bulk-like' spatial correlations near the surface is confounded by the massive gradient in mean relaxation time with distance from the surface. A typical calculation of spatial correlations that involves all three dimensions (or visual analysis of spatial correlations) will be highly biased by this gradient. To circumvent this

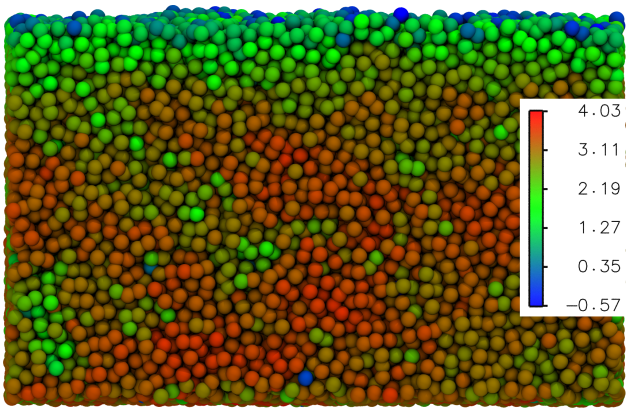

FIG. 6. Side-view of simulated film at T = 0.431, in which beads are colored by their relaxation time, as shown in the color bar (rendered in VMD[55]). All simulated beads are shown. The top of the image corresponds to the free surface, and the bottom of the image corresponds to the substrate-adjacent material.

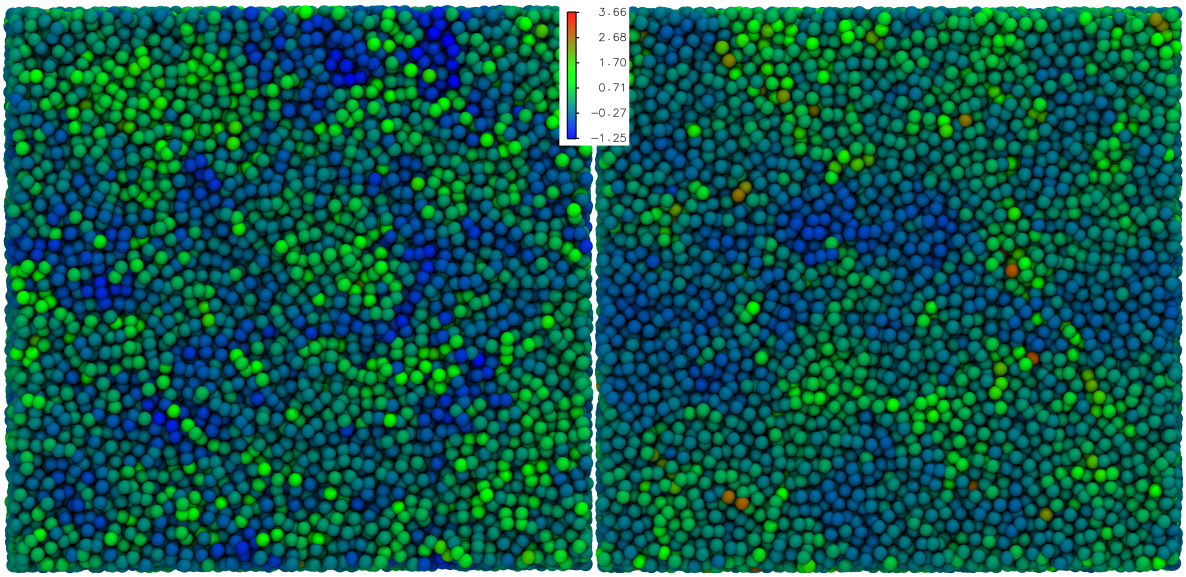

FIG. 7. Simulation image (rendered in VMD) of free surface (left) and a slice of the film at a depth of 20 σ_{LJ} (right). Beads are colored by residual log relaxation time as shown by the color scale.

complication, we compute a residual log relaxation time for each particle i by subtracting from the particle's $\log(\tau)$ value the fit value $\log(\tau_{fit}(z))$ at that z extracted from equation (1), to obtain

$$\delta_i = \log\left(\frac{\tau_i}{\tau_{fit}\left(z\right)}\right). \tag{6}$$

This effectively removes the mean gradient from the data, yielding a quantity that reports

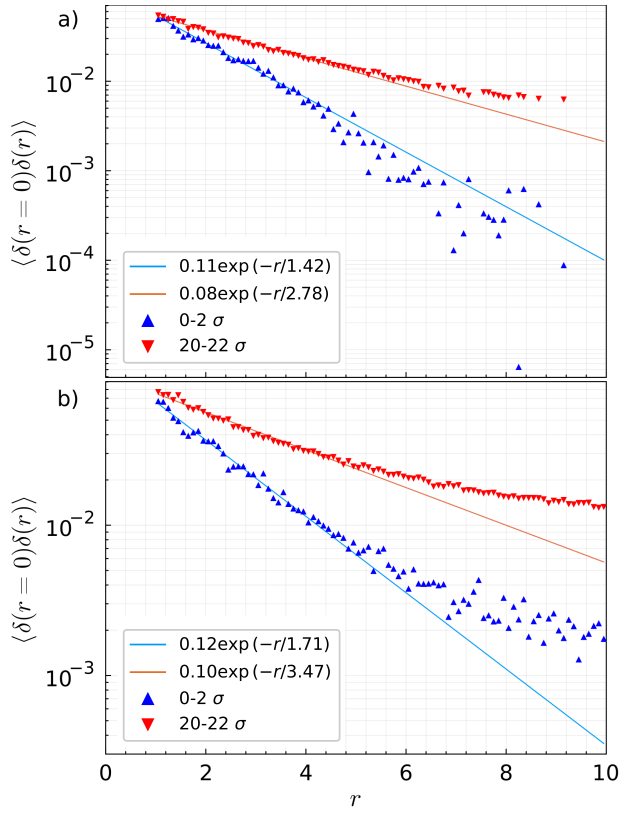

FIG. 8. Cross-correlation function of relaxation time τ residual, for particles near the film surface and deep in the film interior (see legend) at T = 0.450 (top) and T = 0.431 (bottom). Lines are fits of an exponential decay to the correlation over the first 6σ.

the mobility of a given particle relative to the typical mobility at its distance from the surface.

In Figure 7 we show a face-on image of the surface of the film and of a cross section in the middle of the film, in which each bead is colored by its relaxation time residual δ. Two aspects of the heterogeneity are perceptible in these images. First, the broader distribution of relaxation times at the free surface that was quantitatively demonstrated above is qualitatively visible here in the broader color range at the surface as compared to the interior (note the more vibrant coloration on the blue, or faster, end of the spectrum). At the same time, these images suggest a new feature that cannot be captured by the distribution plots above: the distribution of relaxation times appears to more spatially organized in the midfilm, even though the surface is more spatially heterogeneous as measured by the breadth of the distribution.

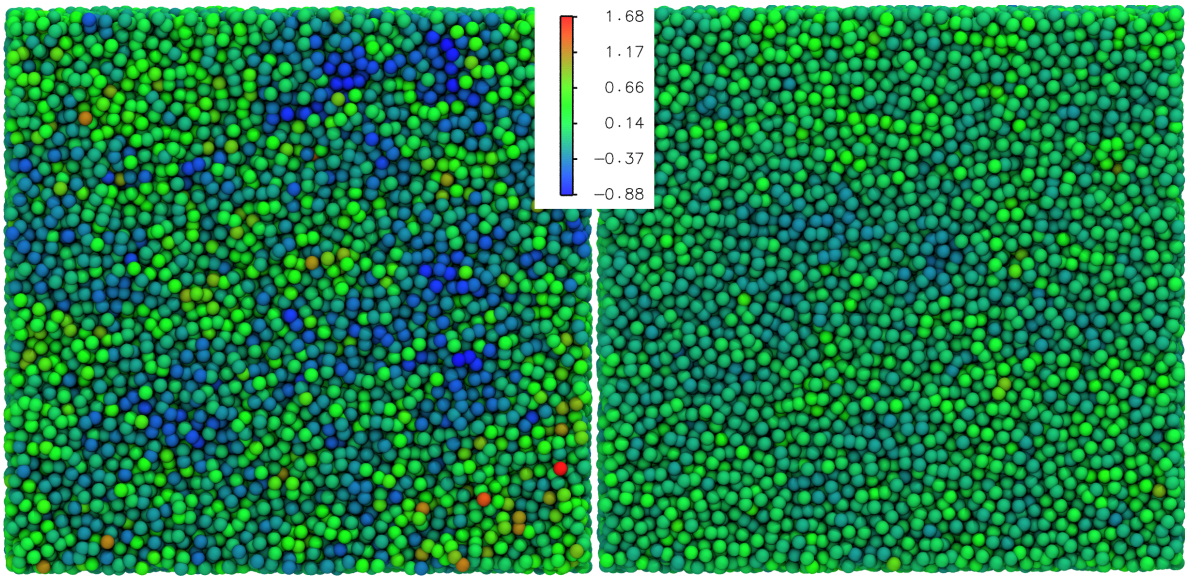

FIG. 9. Simulation image (rendered in VMD) of free surface (left) and a slice of the film at a depth of 20 σ_{LJ} (right). Beads are colored by residual log displacement time t^* as shown by the color scale.

To better quantify this spatial organization, we define a $\delta - \delta$ radial correlation function as

$$C_\tau(r) = \langle \delta(r=0)\delta(r) \rangle, \tag{7}$$

where $\delta(r=0)$ refers to some arbitrarily chosen central particle, r denotes the distance from this central particle, and the brackets denote an average of this calculation over all central particles within a bin of particles at distance z from the surface. In Figure 8 we plot this correlation function for particles within the upper 2σ of the film and for particles in a 2σ slab deep in the film, corresponding to the planes shown in Figure 7. This figure confirms that residual mobility correlations are both stronger and longer-ranged in the mid-film than at the surface. Indeed, at the surface $C_\tau(r)$ has a decorrelation range of 1.42 σ and 1.72 σ at T = 0.450 and T = 0.432, respectively, while in the midfilm it has the longer range of 2.78 σ and 3.47 σ at T = 0.450 and T = 0.432, respectively.

This interpretation is further supported by analysis of the displacement timescale t^*. Figure 9 shows a snapshot of the surface and of a plane at 20 σ from the surface as before, but in this case colored by the residual of t^*. Here the much larger distribution breadth at the surface is particularly clear visually (it is more visually apparent than in Figure 7 because of the inherently narrower range of the t^* distribution). At the same time, the more spatially

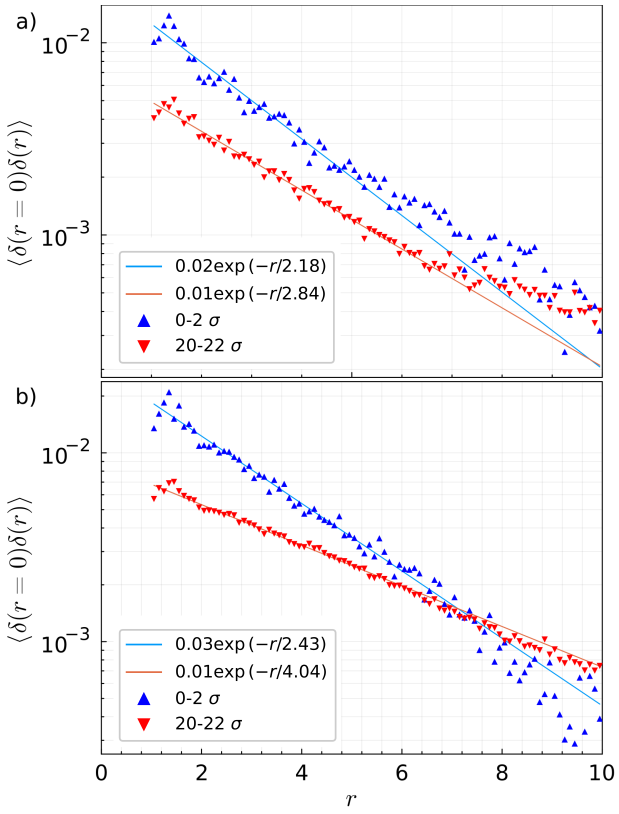

FIG. 10. Cross-correlation function of relaxation time t^* residual, for particles near the film surface and deep in the film interior (see legend) at T = 0.450 (top) and T = 0.431 (bottom). Lines are fits of an exponential decay to the correlation over the first 6σ.

organized character of the heterogeneity in the midfilm remains faintly visible. Residual correlation plots for t^*, shown in Figure 10, again reinforce this at a more quantitative level, with residual t^* cross-correlations exhibiting a shorter range at the free surface than in the mid-film.

These findings add to the nontrivial temperature dependence of surface effects on dynamics and dynamic heterogeneity. In bulk glass-forming liquids, dynamical heterogeneities are expected to become more spatially correlated on cooling[18,19]. Combining the results above, it appears that free surfaces act 'hotter' in terms of their mean relaxation time and spatially correlatedness of relaxation times, but 'colder' in terms of the breadth of the relaxation time distribution.

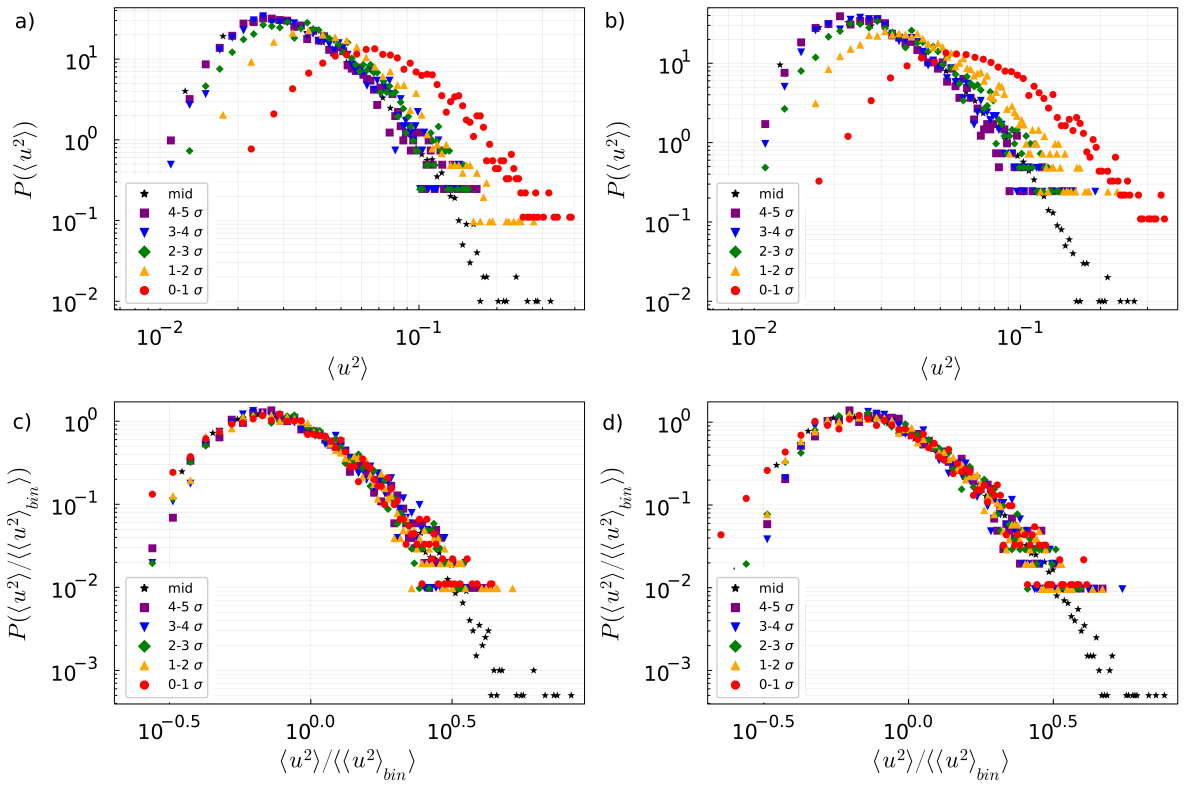

FIG. 11. Distribution of Debye-Waller factors for bins of particles at distances from the free surface noted in the legend. The left column of panels reports data at a temperature T = 0.431 while the right column reports data at a temperature of T = 0.450. Panels (c) and (d) report the same values, but for each particle normalized by the mean value in that bin of particles.

B. Surface modifications of caging heterogeneity

In addition to exhibiting heterogeneity at the level of relaxation times, it has long been known that the segmental caging size scale of glass-forming liquids is heterogeneous as well[17,56,57]. Indeed, evidence suggests that regions with looser caging tend to relax more quickly[17,58], although there is evidence that this relationship locally breaks down near surfaces[46,58,59]. A number of modern theories of glass formation also posit that temperature-variation of the cage scale is a central driver of non-Arrhenius dynamics in glass-formers[50,51,60–64].

Given the above connections between caging and relaxation, it is of natural interest to understand how heterogeneity of the cage scale varies near surfaces in parallel with alterations to relaxation behavior. To assess this, we compute the Debye-Waller factor $\langle u^2 \rangle$, which is a

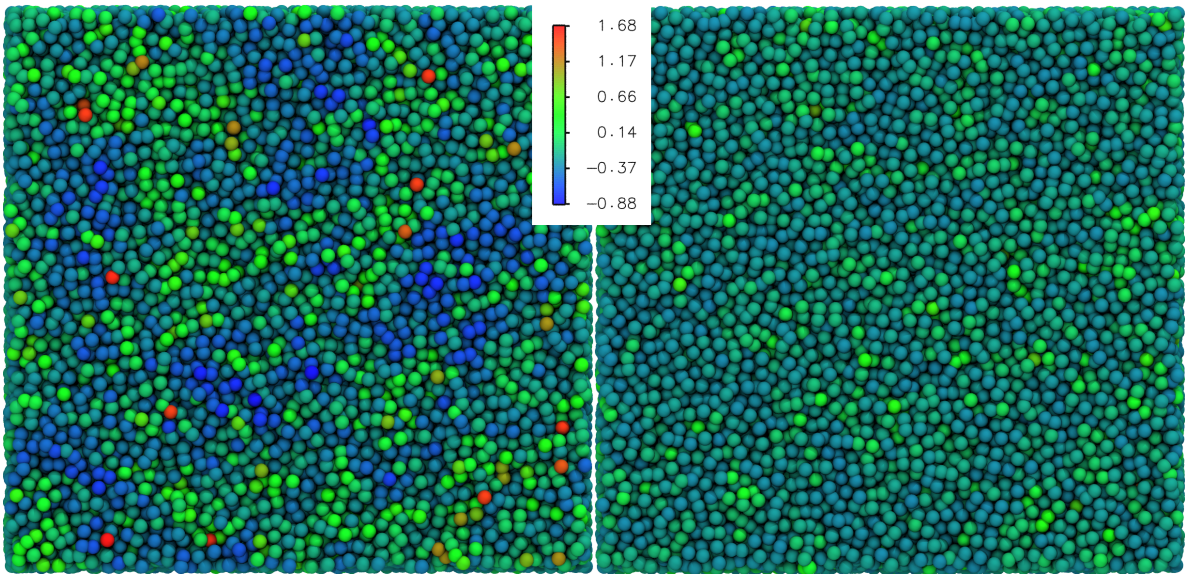

FIG. 12. Simulation image (rendered in VMD) of free surface (left) and a slice of the film at a depth of 20 σ_{LJ} (right). Beads are colored by residual $\langle u^2 \rangle$ as shown by the color scale. Something is wrong here - need to check.

common measure of cage scale and is defined as the value of the mean-square displacement in the caging plateau[33,65–70] $r^2(t = 1\tau_{LJ})\rangle$, consistent with many prior simulation studies.

As shown in Figure 1(e) and (f), the distribution of $\langle u^2 \rangle$ shifts to higher values near the interface, although this effect is evidently much shorter ranged than the gradients in τ and t^*. This is consistent with results of prior studies probing local mean behavior[46,59]. Alterations in the $\langle u^2 \rangle$ distribution near the surface are made clear at a more quantitative level in Figure 11, which shows that a large portion of the distribution simply shifts to higher values upon approach to the interface. There is a modest broadening of the $\langle u^2 \rangle$ distribution proximate to the free surface, but this effect is quite short ranged, apparently dying out with a few σ of the free surface. Moreover, this broadening is largely restricted to the high $\langle u^2 \rangle$ (low inverse $\langle u^2 \rangle$) portion of the distribution.

As with τ and t^*, we compute a residual for $\langle u^2 \rangle$ by subtracting off from each particle $\langle u^2 \rangle$ the interpolated mean gradient value of $\langle u^2 \rangle$ at that z. In this case, we fit the $\langle u^2 \rangle$ gradient to a single-exponential rather than double-exponential form, which is both an empirically better fit and is conceptually reasonable given the standard conception of τ as varying roughly exponentially with inverse $\langle u^2 \rangle$[61,62]. As can be seen in Figure 12, the surface distribution in $\langle u^2 \rangle$ is indeed broader than in the mid-film - this is accentuated here relative

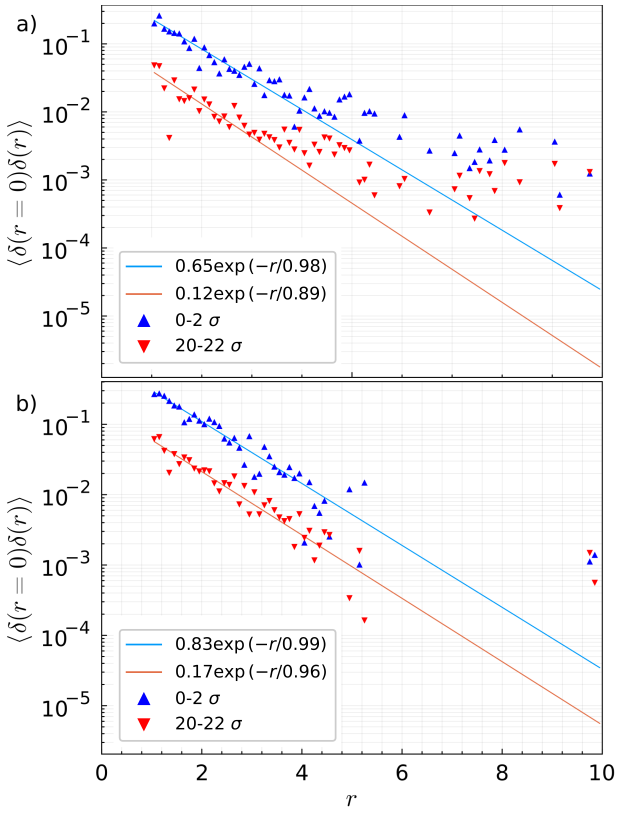

FIG. 13. Cross-correlation function of Debye-Waller factor $\langle u^2 \rangle$ residual, for particles near the film surface and deep in the film interior (see legend) at T = 0.450 (top) and T = 0.431 (bottom). Lines are fits of an exponential decay to the correlation over the first 6σ.

to the distribution broadening visible in Figure 11 due to the logarithmic y-axis in that earlier figure, and the relatively narrow overall distribution of $\langle u^2 \rangle$. This figure also gives a hint that the degree of spatial organization of $\langle u^2 \rangle$ does not vary as strongly near the free surface as is the case for relaxation times. This is shown quantitatively in Figure 13, where it is evident that the decorrelation range for the $\langle u^2 \rangle$ residual is similar at the free surface and in the midfilm and is in the vicinity of 1 σ in both regions at both temperatures studied.

These findings add to a wealth of data indicating that local packing and local $\langle u^2 \rangle$ do not locally control dynamics near polymer interfaces[46,58,59]. In multiple respects, the gradient in $\langle u^2 \rangle$ behaves in a qualitatively different manner than does the gradient in τ or t^*: $\langle u^2 \rangle$ gradients are shorter ranged; the distribution of $\langle u^2 \rangle$ does not broaden as much at the free surface as do the distributions of τ and t^*; the degree of spatial correlations of $\langle u^2 \rangle$ heterogeneities is not appreciably altered near the free surface (and is relatively temperature-

insensitive) whereas correlations in in τ and t^* decay more rapidly in the free surface than in the bulk-like midfilm. At the same time, multiple studies have suggested that $\langle u^2 \rangle$ is altered by[44,71,72] and perhaps plays a role in mediating[3,73,74] interfacial effects, even if not at the level of local control.

This lack of an intimate local connection between $\langle u^2 \rangle$ and τ near the free surface may be consistent with the most empirically successful theoretical framework in predicting simulated dynamical gradients near free surfaces[31,75–78] — the Elastically Cooperative Nonlinear Langevin Equation theory[63,64]. This theory predicts that both gradients in $\langle u^2 \rangle$ and longer ranged collective elastic effects play complementary roles in controlling alterations in τ over the first $\sim$ 10 nm near free surfaces. Because of this convolution of two distinct (but related) mechanisms of dynamical alteration near the interface, a precise local correspondence of τ and $\langle u^2 \rangle$ variations near the free surfaces is not expected, and indeed τ gradients are predicted to be longer-ranged than $\langle u^2 \rangle$ gradients[31]. No predictions have yet been made regarding the spatial heterogeneity of $\langle u^2 \rangle$ vs τ near interfaces via this theoretical framework. The present findings may thus provide an additional empirical target for testing this and other theories of dynamical alterations near interfaces.

C. Dynamical anisotropy at the free surface

Finally, some prior studies probing dynamics near interfaces have suggested that nontrivial dynamical anisotropy effects may emerge near glass-forming liquid interfaces[59,79,80]. For example, Hanakata et al. reported differential alterations of in-plane vs out-of-plane dynamics near atomistically smooth interfaces[59]. Our current dataset enables a unique probe of whether anisotropic dynamics emerge near free surfaces. As shown by Figure 14, there is an indication of an emergence of a slow-relaxing population of particles (relative to other near-surface particles) at the free surface in the normal direction only. This feature, visible in Figure 14(c) and (d) for normal-direction relaxation but not in 14(a) and (b) for in-plane relaxation, suggests the presence of a short-ranged anisotropy at the film surface. As shown in Figure 15(c) and (d), no comparably appreciable anisotropy is present in $\langle u^2 \rangle$ at the free surface. Instead, this anistropy emerges in displacements at increasing times. As shown by Figure 15(a) and (b), a significant population of low-displacement surface particles emerges at long times for displacement in the normal direction, but not in-plane direction, near the

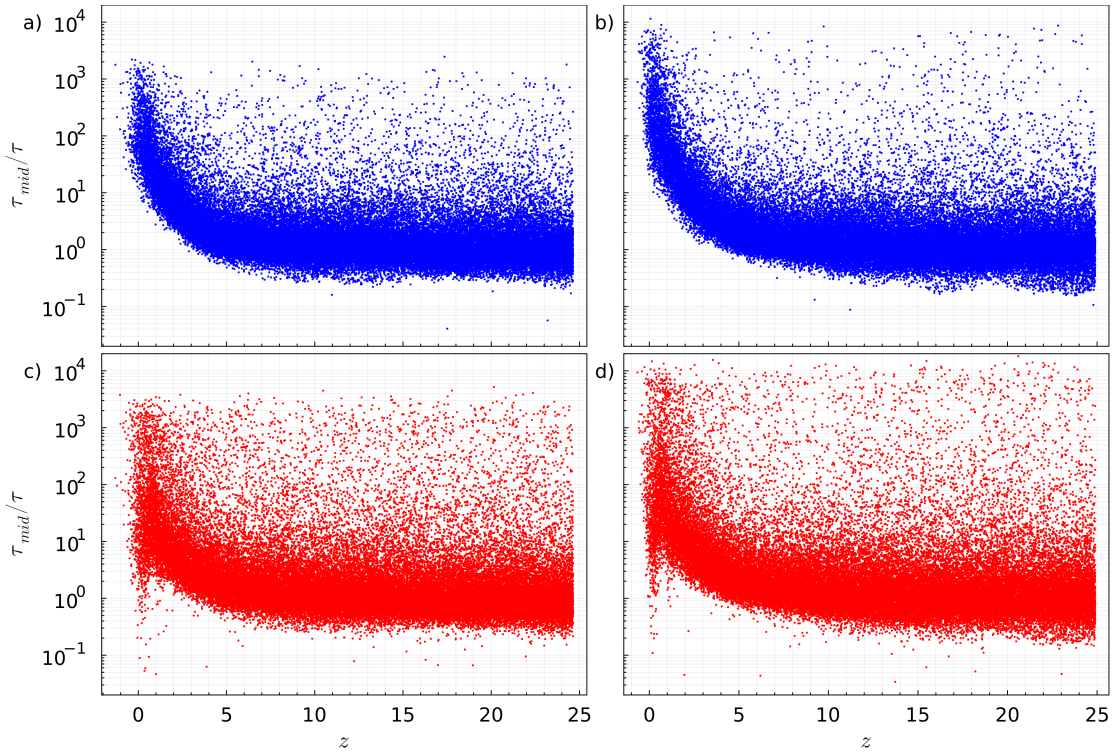

FIG. 14. In plane (top panels) and out of plane (bottom panels) segmental relaxation times of all particles in the upper 25 σ of the film as a function of distance from the surface. The left column of panels reports data at a temperature T = 0.431 while the right column reports data at a temperature of T = 0.450.

free surface.

We can quantify these trends more clearly by separately averaging normal and in-plane displacements of particles in bins at varying distances for the free surface and at varying times of displacement. As shown in Figure 16, a local dip in the normal displacement near the free surface emerges at long times with increasing displacement timescale. As can be seen in this figure, this dip occurs nearly at the location where the density drops off near the surface. We emphasize that this effect is not a consequence of any density layering, since none is present at the free surface. This effect is also largely absent at shorter times associated with the mean alpha relaxation time of the system or less. This can be seen in the alpha relaxation time gradients in 14, which lack this minimum, in the Debye-Waller factor gradients shown in 15 c and d, and in the shorter-time data in 16 a and b. The nonmonotonicity instead emerges only at longer timescales over which particles have on average relaxed multiple times. Along with our relatively high spatial resolution, this explains why this nonmonotonicity was not

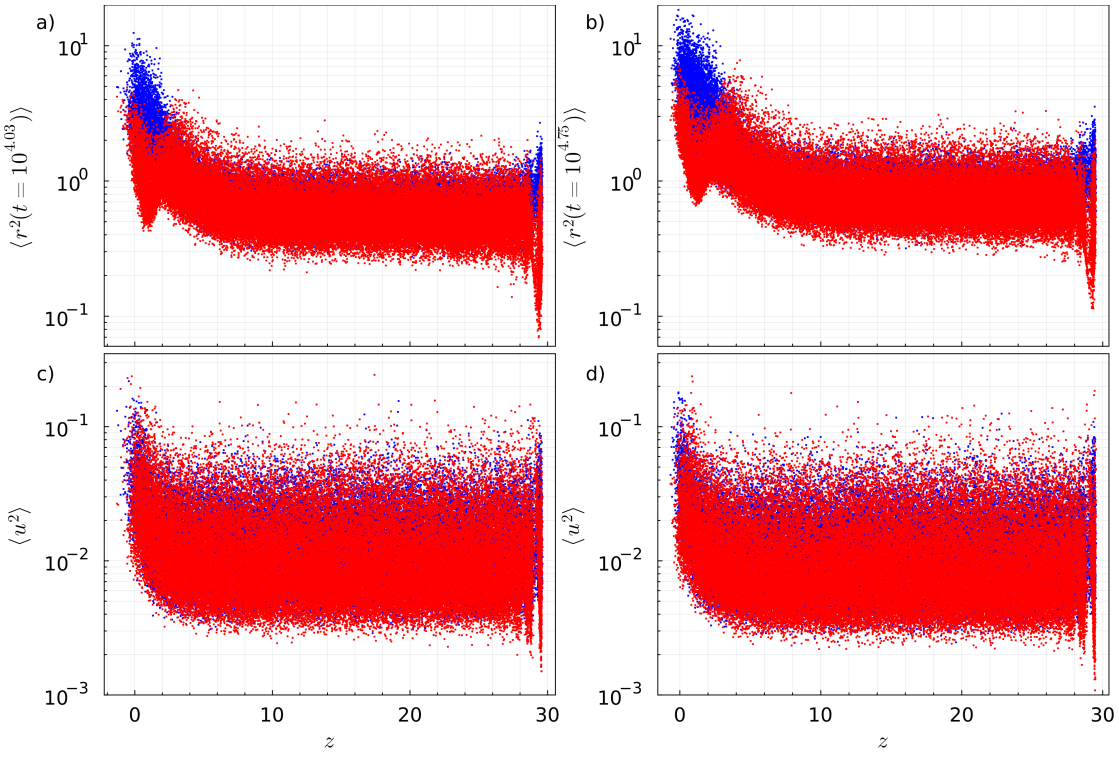

FIG. 15. (a and b) Per-particle mean-square displacement at a time of $10^{4.3}\tau_{LJ}$ as a function of distance from the surface, with red points denoting displacement normal to the surface and blue points displacement parallel to the surface. (c and d) Debye-Waller factor, corresponding to mean-square displacment at a time of $10^{0}\tau_{LJ}$ as a function of distance from the surface, with red points denoting displacement normal to the surface and blue points displacement parallel to the surface. Left panels (a and c) report data at a temperature of T = 0.431, while right panels report data at a temperature of T = 0.450

observed in prior studies that focused on anisotropy in gradients in the alpha time itself[59].

This long-time emergence in the diffusive regime, combined with the non-monotonic character of the anisotropy, suggests a physical origin of this effect in the effective reflective boundary condition imposed by the free surface. Particles approximately one segmental diameter from the free surface can initially displace either towards or away from the surface over a length scale of their own diameter. However, the particles that displace towards the surface must, on average, reverse direction and return to their starting value of z over larger timescales, due to the strict boundary imposed by the film surface. This necessarily recursive behavior for displacements in the +z direction reduces the mean normal displacement of

these particles over intermediate timescales in the diffusive regime. By contrast, particles that are at the absolute upper limit of the surface (i.e. well into the gradient of decreasing density in the +z direction) cannot appreciably displace in the +z direction at all due to their cohesive interactions with the film beneath them; the recursion effect is thus absent, and normal-direction dynamics are accelerated in a manner similar to in-plane dynamics due to the dynamical gradient. This observed anisotropy is similar to that observed in prior work probing dynamics near repulsive atomistically smooth walls. Such walls yield dynamical gradients similar to those near free surfaces[36]; however, the strong reflecting behavior imposed by an explicit wall way make this anisotropy more readily amenable to observation at shorter times than at free surfaces. Finally, we note that, as shown in 16(c) and (d), the in-plane displacement behavior is dominant in determining the isotropic mean square displacement at the free surface, both because it reflects two of the three degrees of freedom in the isotropic quantity, and because the linear arithmetic average is weighted towards larger values when plotted on a logarithmic scale.

While this study focuses most heavily on behavior at the free surface, Figure 16 provides an interesting insight into anisotropic dynamics at the substrate. As discussed in the methods section, this substrate employs a polymer-wall interaction energy selected in prior work[31] to be nearly dynamically neutral, in the sense that it yields almost bulk-like dynamics near the substrate. Figure 16 suggests that this occurs via a cancellation of opposing effects on in-plane and out-of-plane dynamics: in-plane dynamics are modestly accelerated, while normal dynamics are suppressed. We suggest the following scenario for why this occurs. The presence of a local suppression of normal dynamics even near a free surface suggests that this effect is likely relatively insensitive to polymer–wall interaction, since it emerges mainly from the reflecting nature of the boundary condition. Such a condition is implied at any thermodynamically sharp interface. By contrast, in-plane mobility at the substrate is strongly tuned by substrate interaction, because the attraction strength tunes the depth of attractive wells at the substrate and effectively tunes the roughness of the potential energy landscape for in-plane motion. Dynamic neutrality thus occurs when the in-plane mobility enhancement is tuned to cancel out the reflective normal-direction mobility suppression.

This scenario suggests the potential for a fascinating decoupling in properties near solid substrates. Substrates that are nearly dynamically neutral from the perspective of segmental dynamics and T_g will likely tend to produce a modest enhancement of in-plane diffusional

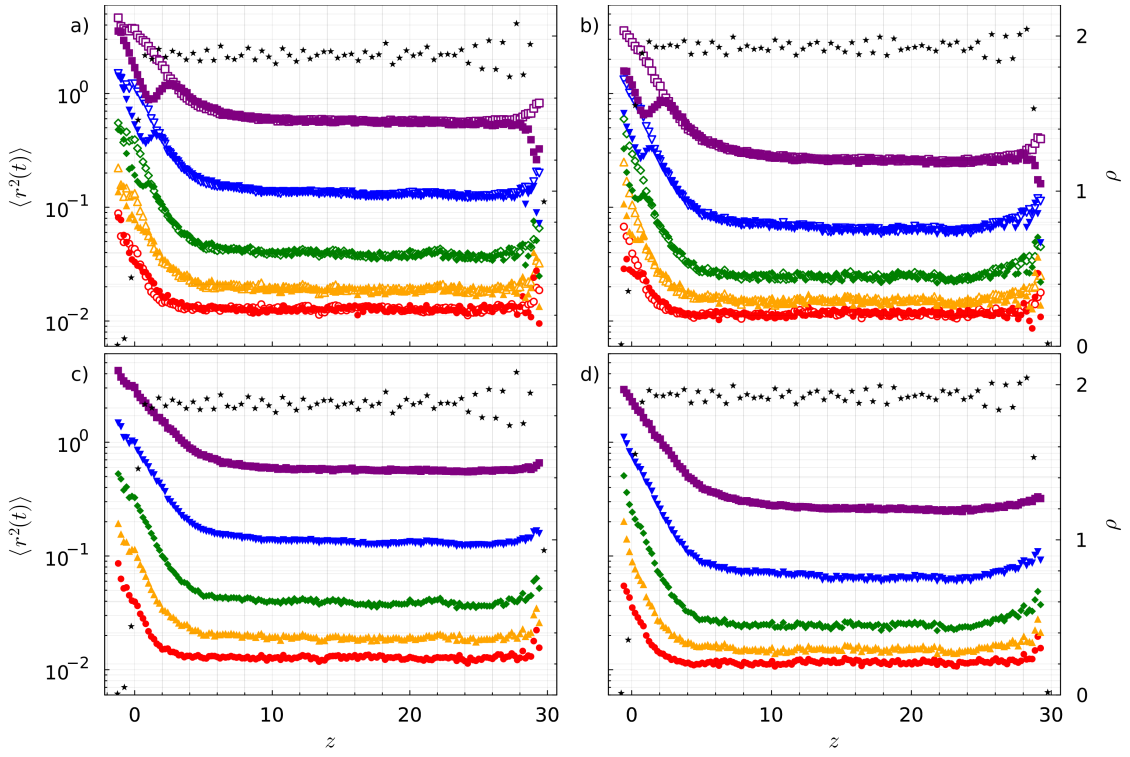

FIG. 16. Colored symbols (left axis) report mean square displacement, averaged over particles in narrow bins of distance z from the surface. Upper panels a) and b) report in-plane mean-square displacement (open symbols) and out-of-plane mean-square displacement (filled symbols. Lower panels c) and d) report isotropic mean-square displacements. Data are reported at multiple displacement times of $10^0\tau_{LJ}$ (red circles), $10^1\tau_{LJ}$ (orange upwards triangles), $10^2\tau_{LJ}$ (green diamonds), $10^3\tau_{LJ}$ (blue downward triangles), $10^4\tau_{LJ}$ (purple squares). Black stars (right axis) denote the number density as a function of distance from the right surface. The left column of panels reports data at a temperature $T = 0.431$ while the right column reports data at a temperature of $T = 0.450$.

rates, since the former is subject to the in-plane/out-of-plane compensation effect, whereas the latter is primarily sensitive to the in-plane effect. In concert with the finding above to the effect that slower dynamics are altered over a greater range than faster dynamics, this provides an additional mechanism by which distinct dynamical properties may become decoupled under nanoconfinement.

IV. CONCLUSIONS

Our results point to a complex interplay between the dynamic heterogeneity that is present in a bulk glass and the immense spatial gradient in dynamics that exists at the surface of glass-forming liquids. Within this surface gradient, the in-plane distribution of relaxation times broadens, in addition to the normal-direction broadening innately associated with the presence of a dynamical gradient. At the same time, the distribution of relaxation times becomes less spatially correlated near the surface. This scenario is in contrast to bulk glass-forming liquids, where reductions in relaxation time (with increasing temperature), *narrowing* of the relaxation time spectrum, and decreased spatial correlations all track together.

Prior studies have reported evidence that the relaxation spectrum of confined glass-forming liquids, *when averaged over the entire material* broadens relative to bulk[81–89]. That type of mean-response broadening is required by necessity in the presence of a large gradient of dynamics, since the gradient itself corresponds to a massive dynamical heterogeneity and thus broadening of the spectrum. Notably, our finding here is quite distinct and not required by those present findings: we find that the *local* heterogeneity near the surface within the gradient increases, even if heterogeneity is effectively assessed at an in-plane level without appreciable contributions from gradient averaging.

We additionally find that the surface has a differential impact on distinct components of the relaxation spectrum, with slower-relaxing components of the spectrum altered over a larger distance from the interface than faster-relaxing components. This implies a differing dynamical impact of the surface on dynamical quantities that probe distinct moments of the relaxation spectrum, a result that may shed light on frequently discordant measurements of nanoconfinement effects by distinct methods. Abetting this effect, we find that the surface induces a distinct short-ranged dynamical *anisotropy*, wherein in-plane displacement occurs more rapidly than out of plane displacement. We show that, at a substrate, this can lead to a scenario in which segmental relaxation times are bulk-like, but in-plane mobility is enhanced. This may also contribute to qualitative and quantitative differences in the impact of a given interface on distinct dynamical quantities.

At least at the temperatures probed in this study, the magnitudes of the surface gradient and of the bulk-like heterogeneous distribution of relaxation times are roughly comparable.

The mean relaxation time at the surface is approximately 2 orders of magnitude smaller than in the mid-film (see Figure 4), while the mid-film relaxation time distribution is perhaps 1-2 orders of magnitude in breadth depending on how it is measured (see Figure 2 and Figure 3). This leaves open the question of whether the breadth of the bulk dynamically hereogeneous distribution and the magnitude of the surface gradient may be linked in some deep manner. A resolution of this question will require simulations of this kind over many temperatures and extending to larger mean relaxation times, allowing quantitative assessment of the extent to which these phenomenon track together on cooling. Because of the high computational cost of isoconfigurational simulations, this will be extremely challenging and require a much larger order computational effort. However, it should be a priority in future simulation work.

ACKNOWLEDGMENTS

This material was based upon work supported by the National Science Foundation under Grant No. CBET – 2208238.

REFERENCES

[1]C. B. Roth, "Polymers under nanoconfinement: where are we now in understanding local property changes?" Chemical Society Reviews **50**, 8050–8066 (2021), publisher: Royal Society of Chemistry.

[2]K. S. Schweizer and D. S. Simmons, "Progress towards a phenomenological picture and theoretical understanding of glassy dynamics and vitrification near interfaces and under nanoconfinement," Journal of Chemical Physics **151**, 240901 (2019).

[3]D. S. Simmons, "An Emerging Unified View of Dynamic Interphases in Polymers," Macromolecular Chemistry and Physics **217**, 137–148 (2016).

[4]M. D. Ediger and J. A. Forrest, "Dynamics near Free Surfaces and the Glass Transition in Thin Polymer Films: A View to the Future," Macromolecules **47**, 471–478 (2014).

[5]D. Cangialosi, V. M. Boucher, A. Alegria, and J. Colmenero, "Physical aging in polymers and polymer nanocomposites: recent results and open questions," Soft Matter **9**, 8619–8630 (2013).

[6]R. Richert, "Dynamics of Nanoconfined Supercooled Liquids," Annual Review of Physical Chemistry **62**, 65–84 (2011).

[7]G. B. McKenna, "Ten (or more) years of dynamics in confinement: Perspectives for 2010," The European Physical Journal Special Topics **189**, 285–302 (2010).

[8]C. B. Roth and J. R. Dutcher, "Glass transition and chain mobility in thin polymer films," Journal of Electroanalytical Chemistry **584**, 13–22 (2005).

[9]J. Baschnagel and F. Varnik, "Computer simulations of supercooled polymer melts in the bulk and in confined geometry," Journal of Physics: Condensed Matter **17**, R851–R953 (2005).

[10]M. Alcoutlabi and G. B. McKenna, "Effects of confinement on material behaviour at the nanometre size scale," Journal of Physics: Condensed Matter **17**, R461–R524 (2005).

[11]J. A. Forrest and K. Dalnoki-Veress, "The glass transition in thin polymer films," Advances in Colloid and Interface Science **94**, 167–195 (2001).

[12]R. Yamamoto and A. Onuki, "Dynamics of highly supercooled liquids: Heterogeneity, rheology, and diffusion," Physical Review E **58**, 3515–3529 (1998).

[13]G. S. Matharoo, M. S. G. Razul, and P. H. Poole, "Structural and dynamical heterogeneity in a glass-forming liquid," Physical Review E **74**, 050502 (2006).

[14]A. Widmer-Cooper and P. Harrowell, "Predicting the Long-Time Dynamic Heterogeneity in a Supercooled Liquid on the Basis of Short-Time Heterogeneities," Physical Review Letters **96**, 185701 (2006).

[15]K. Paeng and L. J. Kaufman, "Single Molecule Experiments Reveal the Dynamic Heterogeneity and Exchange Time Scales of Polystyrene near the Glass Transition," Macromolecules **49**, 2876–2885 (2016), publisher: American Chemical Society.

[16]M. D. Ediger, "Spatially Heterogeneous Dynamics in Supercooled Liquids," Annual Review of Physical Chemistry **51**, 99–128 (2000).

[17]H. Tanaka, T. Kawasaki, H. Shintani, and K. Watanabe, "Critical-like behavior of glass-forming liquids," Nature Materials **9**, 324–331 (2010).

[18]F. W. Starr, J. F. Douglas, and S. Sastry, "The relationship of dynamical heterogeneity to the Adam-Gibbs and random first-order transition theories of glass formation," The Journal of Chemical Physics **138**, 12A541–12A541–18 (2013).

[19]F. H. M. Zetterling, M. Dzugutov, and S. I. Simdyankin, "Formation of large-scale icosahedral clusters in a simple liquid approaching the glass transition," Journal of Non-Crystalline

Solids **293**, 39–44 (2001).

[20]D. Diaz Vela and D. S. Simmons, "The microscopic origins of stretched exponential relaxation in two model glass-forming liquids as probed by simulations in the isoconfigurational ensemble," The Journal of Chemical Physics **153**, 234503 (2020).

[21]M. T. Cicerone, F. R. Blackburn, and M. D. Ediger, "How do molecules move near Tg? Molecular rotation of six probes in o-terphenyl across 14 decades in time," The Journal of Chemical Physics **102**, 471 (1995).

[22]J. P. Garrahan and D. Chandler, "Geometrical explanation and scaling of dynamical heterogeneities in glass forming systems," Physical Review Letters **89**, 035704 (2002).

[23]D. Chandler and J. P. Garrahan, "Dynamics on the way to forming glass: Bubbles in space-time," Annual Review of Physical Chemistry **61**, 191–217 (2010).

[24]A. Zhang, A. R. Moore, H. Zhao, S. Govind, S. E. Wolf, Y. Jin, P. J. Walsh, R. A. Riggleman, and Z. Fakhraai, "The role of intramolecular relaxations on the structure and stability of vapor-deposited glasses," The Journal of Chemical Physics **156**, 244703 (2022).

[25]N. B. Tito, J. E. G. Lipson, and S. T. Milner, "Lattice model of mobility at interfaces: free surfaces, substrates, and bilayers," Soft Matter **9**, 9403–9413 (2013).

[26]J. DeFelice, S. T. Milner, and J. E. G. Lipson, "Simulating local tg reporting layers in glassy thin films," Macromolecules (2016), 10.1021/acs.macromol.6b00090.

[27]D. Long and F. Lequeux, "Heterogeneous dynamics at the glass transition in van der waals liquids, in the bulk and in thin films," The European Physical Journal E **4**, 371–387 (2001).

[28]L. Berthier, "Self-induced heterogeneity in deeply supercooled liquids," arXiv:2010.12244 [cond-mat, physics:physics] (2020), arXiv: 2010.12244.

[29]K. Kremer and G. S. Grest, "Dynamics of entangled linear polymer melts: A molecular-dynamics simulation," The Journal of Chemical Physics **92**, 5057–5086 (1990).

[30]M. E. Mackura and D. S. Simmons, "Enhancing heterogenous crystallization resistance in a bead-spring polymer model by modifying bond length," Journal of Polymer Science Part B: Polymer Physics **52**, 134–140 (2014).

[31]A. Ghanekarade, A. D. Phan, K. S. Schweizer, and D. S. Simmons, "Signature of collective elastic glass physics in surface-induced long-range tails in dynamical gradients," Nature Physics , 1–7 (2023).

[32]S. J. Plimpton, "Fast parallel algorithms for short-range molecular dynamics," J. Comp. Phys. **117**, 1–19 (1995).

[33]J.-H. Hung, T. K. Patra, V. Meenakshisundaram, J. H. Mangalara, and D. S. Simmons, "Universal localization transition accompanying glass formation: insights from efficient molecular dynamics simulations of diverse supercooled liquids," Soft Matter **15**, 1223–1242 (2018).

[34]J. A. Forrest, "What can we learn about a dynamical length scale in glasses from measurements of surface mobility?" The Journal of Chemical Physics **139**, 084702 (2013).

[35]J. A. Forrest and K. Dalnoki-Veress, "When Does a Glass Transition Temperature Not Signify a Glass Transition?" ACS Macro Letters **3**, 310–314 (2014).

[36]P. Scheidler, W. Kob, and K. Binder, "The relaxation dynamics of a confined glassy simple liquid," European Physical Journal E **12**, 5–9 (2003), wOS:000186890400002.

[37]P. Scheidler, W. Kob, and K. Binder, "Cooperative motion and growing length scales in supercooled confined liquids," Europhysics Letters (EPL) **59**, 701–707 (2002).

[38]Y. Li, W. Zhang, C. Bishop, C. Huang, M. D. Ediger, and L. Yu, "Surface diffusion in glasses of rod-like molecules posaconazole and itraconazole: effect of interfacial molecular alignment and bulk penetration," Soft Matter **16**, 5062–5070 (2020), publisher: The Royal Society of Chemistry.

[39]D. Diaz-Vela, J.-H. Hung, and D. S. Simmons, "Temperature-Independent Rescaling of the Local Activation Barrier Drives Free Surface Nanoconfinement Effects on Segmental-Scale Translational Dynamics near Tg," ACS Macro Letters **7**, 1295–1301 (2018).

[40]D. Vela, A. Ghanekarade, and D. S. Simmons, "Probing the Metrology and Chemistry Dependences of the Onset Condition of Strong "Nanoconfinement" Effects on Dynamics," Macromolecules **53**, 4158–4171 (2020).

[41]S. Peter, H. Meyer, J. Baschnagel, and R. Seemann, "Slow dynamics and glass transition in simulated free-standing polymer films: a possible relation between global and local glass transition temperatures," Journal of Physics-Condensed Matter **19**, 205119 (2007), wOS:000246567700020.

[42]R. Priestley, D. Cangialosi, and S. Napolitano, "On the equivalence between the thermodynamic and dynamic measurements of the glass transition in confined polymers," Journal of Non-Crystalline Solids **407**, 288–295 (2015).

[43]J. H. Mangalara, M. E. Mackura, M. D. Marvin, and D. S. Simmons, "The relationship between dynamic and pseudo-thermodynamic measures of the glass transition temperature in nanostructured materials," The Journal of Chemical Physics **146**, 203316 (2017).

[44]C. Ye, C. G. Weiner, M. Tyagi, D. Uhrig, S. V. Orski, C. L. Soles, B. D. Vogt, and D. S. Simmons, "Understanding the Decreased Segmental Dynamics of Supported Thin Polymer Films Reported by Incoherent Neutron Scattering," Macromolecules **48**, 801–808 (2015).

[45]J. E. Pye, K. A. Rohald, E. A. Baker, and C. B. Roth, "Physical Aging in Ultrathin Polystyrene Films: Evidence of a Gradient in Dynamics at the Free Surface and Its Connection to the Glass Transition Temperature Reductions," Macromolecules **43**, 8296–8303 (2010).

[46]R. J. Lang and D. S. Simmons, "Interfacial Dynamic Length Scales in the Glass Transition of a Model Freestanding Polymer Film and Their Connection to Cooperative Motion," Macromolecules **46**, 9818–9825 (2013).

[47]S. Kim, S. A. Hewlett, C. B. Roth, and J. M. Torkelson, "Confinement effects on glass transition temperature, transition breadth, and expansivity: Comparison of ellipsometry and fluorescence measurements on polystyrene films," The European Physical Journal E **30**, 83–92 (2009).

[48]J. E. G. Lipson and S. T. Milner, "Percolation model of interfacial effects in polymeric glasses," The European Physical Journal B **72**, 133–137 (2009).

[49]C. Rotella, M. Wübbenhorst, and S. Napolitano, "Probing interfacial mobility profiles via the impact of nanoscopic confinement on the strength of the dynamic glass transition," Soft Matter **7**, 5260–5266 (2011).

[50]S. Mirigian and K. S. Schweizer, "Communication: Slow relaxation, spatial mobility gradients, and vitrification in confined films," The Journal of Chemical Physics **141**, 161103 (2014).

[51]S. Mirigian and K. S. Schweizer, "Theory of activated glassy relaxation, mobility gradients, surface diffusion, and vitrification in free standing thin films," The Journal of Chemical Physics **143**, 244705 (2015).

[52]M. T. Cicerone, P. A. Wagner, and M. D. Ediger, "Translational Diffusion on Heterogenous Lattices: A Model for Dynamics in Glass Forming Materials," J. Phys. Chem. B **101**, 8727–8734 (1997).

[53]J.-H. Hung, J. H. Mangalara, and D. S. Simmons, "Heterogeneous Rouse Model Predicts Polymer Chain Translational Normal Mode Decoupling," Macromolecules **51**, 2887–2898 (2018).

[54]A. P. Sokolov and K. S. Schweizer, "Resolving the Mystery of the Chain Friction Mecha-

nism in Polymer Liquids," Physical Review Letters **102**, 248301 (2009).

[55]W. Humprey, A. Dalke, and K. Schulten, "Vmd - visual molecular dynamics," Journal of Molecular Graphics **14**, 33–38 (1996).

[56]R. A. Riggleman, J. F. Douglas, and J. J. de Pablo, "Antiplasticization and the elastic properties of glass-forming polymer liquids," Soft Matter **6**, 292–304 (2010).

[57]D. S. Simmons and J. F. Douglas, "Nature and interrelations of fast dynamic properties in a coarse-grained glass-forming polymer melt," Soft Matter **7**, 11010–11020 (2011).

[58]D. M. Sussman, S. S. Schoenholz, E. D. Cubuk, and A. J. Liu, "Disconnecting structure and dynamics in glassy thin films," Proceedings of the National Academy of Sciences **114**, 10601–10605 (2017).

[59]Paul Z. Hanakata, Jack F. Douglas, and Francis W. Starr, "Local Variation of Fragility and Glass Transition Temperature of Ultra-thin Supported Polymer Films," Journal of Chemical Physics **137**, 244901 (2012).

[60]J. C. Dyre, "Colloquium: The glass transition and elastic models of glass-forming liquids," Reviews of Modern Physics **78**, 953–972 (2006).

[61]U. Buchenau and R. Zorn, "A RELATION BETWEEN FAST AND SLOW MOTIONS IN GLASSY AND LIQUID SELENIUM," Europhysics Letters **18**, 523–528 (1992).

[62]R. W. Hall and P. G. Wolynes, "The aperiodic crystal picture and free-energy barriers in glasses," Journal of Chemical Physics **86**, 2943–2948 (1987).

[63]S. Mirigian and K. S. Schweizer, "Elastically cooperative activated barrier hopping theory of relaxation in viscous fluids. I. General formulation and application to hard sphere fluids," Journal of Chemical Physics **140**, 194506 (2014), wOS:000336832700028.

[64]S. Mirigian and K. S. Schweizer, "Elastically cooperative activated barrier hopping theory of relaxation in viscous fluids. II. Thermal liquids," Journal of Chemical Physics **140**, 194507 (2014), wOS:000336832700029.

[65]T. McKenzie-Smith, J. F. Douglas, and F. W. Starr, "Relating dynamic free volume to cooperative relaxation in a glass-forming polymer composite," The Journal of Chemical Physics **157**, 131101 (2022).

[66]F. Puosi, A. Tripodo, and D. Leporini, "Fast vibrational modes and slow heterogeneous dynamics in polymers and viscous liquids," International Journal of Molecular Sciences **20**, 5708 (2019).

[67]B. A. P. Betancourt, P. Z. Hanakata, F. W. Starr, and J. F. Douglas, "Quantita-

tive relations between cooperative motion, emergent elasticity, and free volume in model glass-forming polymer materials," Proceedings of the National Academy of Sciences **112**, 2966–2971 (2015).

[68]A. Ottochian and D. Leporini, "Universal scaling between structural relaxation and caged dynamics in glass-forming systems: Free volume and time scales," Journal of Non-Crystalline Solids **357**, 298–301 (2011).

[69]D. S. Simmons, M. T. Cicerone, Q. Zhong, M. Tyagi, and J. F. Douglas, "Generalized localization model of relaxation in glass-forming liquids," Soft Matter **8**, 11455–11461 (2012).

[70]F. W. Starr, S. Sastry, J. F. Douglas, and S. C. Glotzer, "What do we learn from the local geometry of glass-forming liquids?" Physical Review Letters **89**, 125501 (2002).

[71]C. L. Soles, J. F. Douglas, W.-l. Wu, H. Peng, and D. W. Gidley, "Comparative specular x-ray reflectivity, positron annihilation lifetime spectroscopy, and incoherent neutron scattering measurements of the dynamics in thin polycarbonate films," Macromolecules **37**, 2890–2900 (2004).

[72]R. Inoue, T. Kanaya, K. Nishida, I. Tsukushi, M. T. F. Telling, B. J. Gabrys, M. Tyagi, C. Soles, and W.-l. Wu, "Glass transition and molecular mobility in polymer thin films," Physical Review E **80**, 031802 (2009).

[73]W. Zhang, F. W. Starr, and J. F. Douglas, "Activation free energy gradient controls interfacial mobility gradient in thin polymer films," The Journal of Chemical Physics **155**, 174901 (2021).

[74]D. Ruan and D. S. Simmons, "Roles of chain stiffness and segmental rattling in ionomer glass formation," Journal of Polymer Science Part B: Polymer Physics **53**, 1458–1469 (2015).

[75]A. D. Phan and K. S. Schweizer, "Theory of the spatial transfer of interface-nucleated changes of dynamical constraints and its consequences in glass-forming films," The Journal of Chemical Physics **150**, 044508 (2019).

[76]A. D. Phan and K. S. Schweizer, "Influence of longer range transfer of vapor interface modified caging constraints on the spatially heterogeneous dynamics of glass-forming liquids," Macromolecules **52**, 5192–5206 (2019).

[77]A. D. Phan and K. S. Schweizer, "Theory of spatial gradients of relaxation, vitrification temperature and fragility of glass-forming polymer liquids near solid substrates," ACS

Macro Letters **9**, 448–453 (2020).

[78]A. Ghanekarade, A. D. Phan, K. S. Schweizer, and D. S. Simmons, "Nature of dynamic gradients, glass formation, and collective effects in ultrathin freestanding films," Proceedings of the National Academy of Sciences **118**, e2104398118 (2021).

[79]M. D. Marvin, R. J. Lang, and D. S. Simmons, "Nanoconfinement effects on the fragility of glass formation of a model freestanding polymer film," Soft Matter **10**, 3166–3170 (2014).

[80]F. Varnik, J. Baschnagel, and K. Binder, "Reduction of the glass transition temperature in polymer films: A molecular-dynamics study," Physical Review E **65**, 021507 (2002).

[81]Y. B. Mel'nichenko, J. Schüller, R. Richert, B. Ewen, and C. Loong, "Dynamics of hydrogen-bonded liquids confined to mesopores: A dielectric and neutron spectroscopy study," The Journal of Chemical Physics **103**, 2016–2024 (1995).

[82]P. Pissis, D. Daoukaki-Diamanti, L. Apekis, and C. Christodoulides, "The glass transition in confined liquids," Journal of Physics: Condensed Matter **6**, L325 (1994).

[83]D. Morineau, Y. Xia, and C. Alba-Simionesco, "Finite-size and surface effects on the glass transition of liquid toluene confined in cylindrical mesopores," The Journal of Chemical Physics **117**, 8966–8972 (2002).

[84]M. Arndt, R. Stannarius, H. Groothues, E. Hempel, and F. Kremer, "Length scale of cooperativity in the dynamic glass transition," Physical Review Letters **79**, 2077–2080 (1997).

[85]R. Zorn, L. Hartmann, B. Frick, D. Richter, and F. Kremer, "Inelastic neutron scattering experiments on the dynamics of a glass-forming material in mesoscopic confinement," Journal of Non-Crystalline Solids **307–310**, 547–554 (2002).

[86]Y. Zhang, C. N. Woods, M. Alvarez, Y. Jin, R. A. Riggleman, and Z. Fakhraai, "Effect of substrate interactions on the glass transition and length-scale of correlated dynamics in ultra-thin molecular glass films," The Journal of Chemical Physics **149**, 184902 (2018).

[87]S. Napolitano, E. Glynos, and N. B. Tito, "Glass transition of polymers in bulk, confined geometries, and near interfaces," Reports on Progress in Physics **80**, 036602 (2017).

[88]S. Napolitano and M. Wü"bbenhorst, "Structural relaxation and dynamic fragility of freely standing polymer films," Polymer **51**, 5309–5312 (2010).

[89]J. Schüller, R. Richert, and E. W. Fischer, "Dielectric relaxation of liquids at the surface of a porous glass," Physical Review B **52**, 15232–15238 (1995).